mixture of coarsely ground cooked and uncooked malt. The high proportion of chaff and lack of yeast suggest that these contents are spent grain, that is, the residues that are left after rinsing sugars, dextrins, and starch from processed malt. The large quantities of starch remaining are evidence of the relative inefficiency of the process, but such spent grains may have been re-used to make weaker beer. These findings suggest that fermentation was initiated in the rinsed sugar- and starch-rich liquid obtained after straining out the bulk of cereal husk.

The use of microscopy to investigate macro- and microstructure of desiccated foods has led to new proposals for how ancient Egyptians baked and brewed. The proposals can be tested by experiments in which ancient Egyptian food processing tools and authentic modern cereals (*9*, *21*) are used to replicate the processes described. The replicate foods are now being compared to the ancient specimens by SEM.

The implications of this research extend beyond ancient Egyptian methods of food preparation. Because starch morphology is stable over time in very dry conditions, there is great potential to analyze preparation techniques of other ancient starch-based foods from arid zones throughout the world. Although these regions contain a minority of the global archaeological record, they may serve as a model for ancient food-processing methods in regions where tools and ingredients were similar but organic preservation is much poorer. Microstructural preservation in dry areas is probably not limited to starchy foods. The unique record available from archaeological sites in arid areas provides an important opportunity to explore the development of prepared foods and evolution of food-making technologies.

REFERENCES AND NOTES

1. R. Drenkhahn, in *Lexikon der Aegyptologie. A-Ernte*, W. Helck and E. Otto, Eds. (Otto Harrassowitz, Wiesbaden, Germany, 1975), vol. 1, p. 871.
2. W. Helck, in (*1*), pp. 789–792.
3. C. F. Nims, *J. Egypt. Archaeol.* **44**, 56 (1958).
4. E. Strouhal, *Life in Ancient Egypt* (Cambridge Univ. Press, Cambridge, 1992).
5. H. Wilson, *Egyptian Food and Drink* (Shire Egyptology, Aylesbury, UK, 1988).
6. W. J. Darby, P. Ghalioungui, L. Grivetti, *Food: The Gift of Osiris* (Academic Press, London, 1977), vol. 2.
7. D. Faltings, *Z. Aegypt. Sprache Altertumskunde* **115**, 104 (1991).
8. W. Helck, *Das Bier im Alten Aegypten* (Gesellschaft für die Geschichte und Bibliographie des Brauwesens E.V., Berlin, 1971).
9. D. Samuel, *Cambridge Archaeol. J.* **3**, 276 (1993).
10. L. Wittmack, *Trans. Acad. Sci. St. Louis* **15**, 1 (1905).
11. H. E. Winlock, *The Tomb of Queen Meryet-Amun at Thebes* (Metropolitan Museum, New York, 1932).
12. J. Grüss, *Tagesztg. Brau.* **26**, 1123 (1928); *ibid.* **27**, 275 (1929); *ibid*, p. 517; *ibid.*, p. 679.
13. D. Samuel, *J. Am. Soc. Brew. Chem.* **54**, 3 (1996).
14. ———, *Brew. Guardian* **124**, 26 (1995).
15. R. C. Hoseney, W. A. Atwell, D. R. Lineback, *Cereal Foods World* **22**, 56 (1977).
16. A. Kawabata *et al.*, *Starch* **46**, 463 (1994).
17. G. H. Palmer, *J. Inst. Brew.* **78**, 326 (1972).
18. L. B. Rockland, F. T. Jones, D. M. Hahn, *J. Food Sci.* **42**, 1204, 1212 (1977).
19. B. L. Dronzek, P. Hwang, W. Bushuk, *Cereal Chem.* **49**, 232 (1972).
20. Z. Sun and C. A. Henson, *Plant Physiol.* **94**, 320 (1990).
21. D. Samuel, *Egypt. Archaeol.* **4**, 9 (1994).
22. This work formed part of research for a Ph.D. thesis at the Department of Archaeology, University of Cambridge. It was funded by Scottish and Newcastle Breweries plc and the British Academy and supported by the Egypt Exploration Society. Sampling was carried out with permission of the Ashmolean Museum (Oxford), the British Museum (London), and the Musée du Louvre (Paris). Help was provided by P. Bolt, A. Burgess, C. Bridonneau, B. Chapman, N. Davies, W. V. Davies, P. Echlin, I. Forrest, M. Jones, B. Kemp, R. Mann, J. Merrington, M. Nesbitt, S. Quirke, R. Rose, D. Schofield, M. Serpico, and H. Whitehouse.

16 April 1996; accepted 7 June 1996

Volatiles from the 1994 Eruptions of Rabaul: Understanding Large Caldera Systems

Kurt Roggensack,* Stanley N. Williams, Stephen J. Schaefer,†
Roderic A. Parnell Jr.

The 1994 eruption of Rabaul, in Papua New Guinea, involved a small plinian eruption at Vulcan and a vulcanian eruption on the opposite side of the caldera at Tavurvur. Vulcan's ash leachates indicate seawater interaction that is consistent with earlier observations of low sulfur dioxide emissions and the presence of ice crystals in the initial plinian eruption cloud. In contrast, Tavurvur ash leachates indicate no seawater interaction, and later sulfur dioxide emissions remained high despite low-level eruptive activity. Silicic melt inclusions indicate that the andesitic melt contained about 2 weight percent water and negligible carbon dioxide. Mafic melt inclusions in Tavurvur ash have water and carbon dioxide contents that vary systematically over the course of the eruption. The mafic melt inclusions suggest that a mafic dike intruded from below the silicic chamber and provide further evidence that mafic intrusions drive caldera unrest.

Measurements of volatile elements are critical to our understanding of magmatic and volcanic processes because these elements influence magma evolution and drive explosive eruptions. Large caldera systems, such as Rabaul, in Papua New Guinea, are an important class of volcanoes that are capable of many styles of eruptive behavior. The 1994 eruption of Rabaul, which followed several decades of caldera unrest, provided a unique opportunity to learn more about an active caldera's magmatic system. We measured SO_2 in the eruptive column and H_2O, CO_2, S, and Cl in the eruptive products of the 1994 eruption of Rabaul to provide a temporal record of magmatic volatile concentrations. This record defined the short-lived dynamic processes of Rabaul, which could not be directly observed and are not preserved in the geologic record.

The 1994 eruption involved two volcanoes with different eruptive behavior on opposite sides of the caldera. The initial eruption began at 6:06 a.m. on 19 September 1994 at Tavurvur and gradually gained intensity over a period of 70 min. At 7:17 a.m., the activity shifted primarily to Vulcan, where a new vent on the northern flank produced an ~18- to 20-km-high plinian eruption column and small pyroclastic flows for 70 min. Activity then shifted back to Tavurvur and continued at a much lower intensity, with discrete explosions and an eruption column that reached heights of ~6 km. At the end of September, a small lava flow was noticed in the crater of Tavurvur (*1*). Vulcan produced light tan, highly vesiculated pumice and ash (0.26 km^3) (*1*) with minor scoria. Tavurvur ash (0.04 km^3) (*1*) is dark brown with common scoria and dense glass chips.

Total ozone mapping spectrometer (TOMS) measurements during the first day of the eruption were unable to detect SO_2 in Vulcan's plinian column (*2*, *3*). The low SO_2 content of Vulcan's plinian column and abnormalities in the advanced very high resolution radiometer images of the plinian cloud were attributed to possible seawater interaction and the presence of ice crystals (*2*). On subsequent days, the TOMS detected moderate SO_2 (30 to 80 kton; Fig. 1) in a low-altitude eruption cloud near the caldera that most likely represented the output of Tavurvur. Addition-

K. Roggensack, S. N. Williams, S. J. Schaefer, Department of Geology, Box 871404, Arizona State University, Tempe, AZ 85287–1404, USA.
R. A. Parnell Jr., Department of Geology, Northern Arizona University, Flagstaff, AZ 86011, USA.

---

*To whom correspondence should be addressed.

†Present address: University Space Research Association, NASA/Goddard Space Flight Center, Code 921, Greenbelt, MD 20771, USA.

al measurements of Tavurvur's eruption plume were made with an airborne correlation spectrometer (COSPEC) beginning on 29 September, 10 days after the initial eruption. The SO_2 flux of 26 ± 5 kton/day declined steadily to 4 ± 1 kton/day over a period of 8 days (Fig. 1). No SO_2 release could be detected at Vulcan during this time period and no plume was visible.

Ash leachate analyses provided an indirect method of determining the volatile composition of the eruption columns. Fresh ash samples from Rabaul were collected during the waning stages of the eruption. The ash leachate data (Table 1 and Fig. 2) show a correlation with stratigraphic position and source vent. Early erupted plinian ash from Vulcan was characterized by high Cl and low SO_4, Mg, and F content. These elements are in seawater (*4*) proportions (Cl $\gg SO_4 >$ Mg $\gg$F) but at much lower total abundance. Tavurvur ash, from higher in the stratigraphic section, has higher concentrations of F, SO_4, and Ca than does Vulcan ash, and F and Ca concentrations are substantially higher than in seawater. Ash leachate S/Cl ratios vary over the course of the eruption. Leachates of early erupted Vulcan ash have a S/Cl ratio (0.19) comparable to that of seawater (0.14). In contrast, the majority of Tavurvur ash leachates have high S/Cl ratios (>2) (*5*). Matrix glass (MG) and silicic melt inclusions (MIs) in orthopyroxene and plagioclase from Vulcan and Tavurvur vary over a large compositional range in relation to stratigraphic position (Table 2). The least evolved MIs approach the most evolved whole-rock compositions (59 to 63 weight % SiO_2) (*6*). The silicic MIs have ~2 weight % H_2O (Table 3), high Cl content [2900 to 3900 parts per million (ppm)], and variable S (≤440 ppm).

In addition to minerals typical of high-K andesite (plagioclase, clinopyroxene, orthopyroxene, Fe-Ti oxides, and apatite), the 1994 ash contains a basalt–basaltic andesite mineral assemblage. Olivine, plagioclase, and clinopyroxene aggregates in Tavurvur ash and olivine and plagioclase phenocrysts in Vulcan ash have been suggested

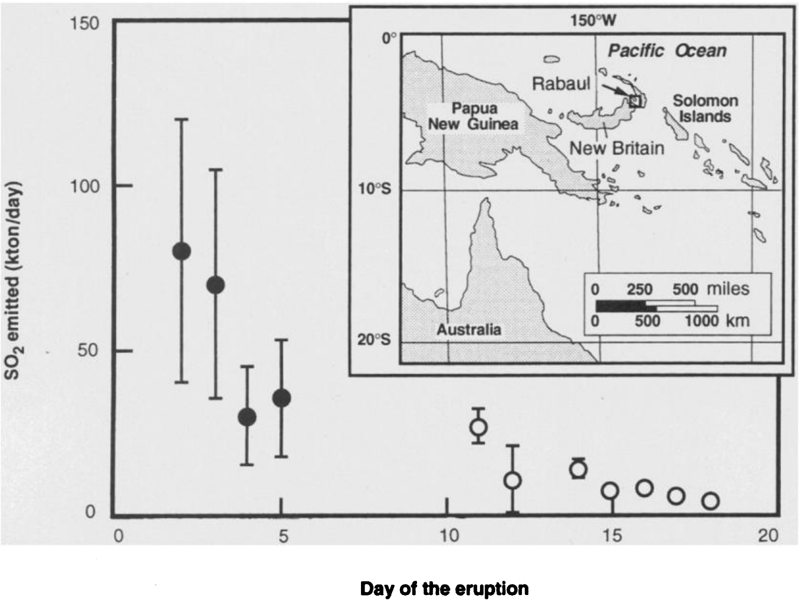

Fig. 1. Sulfur dioxide emissions from the 1994 Rabaul eruption. Data were obtained by TOMS (solid symbols) (*3*) from the low diffuse eruption cloud near the caldera. All other data were obtained by COSPEC (open symbols) analysis of the Tavurvur plume. The inset shows the location of the Rabaul caldera (*17*).

Table 1. Ash leachate data for the 19 September 1994 eruption of Rabaul. Sample preparation follows that in (*19*). Leachate analysis was done by atomic absorption spectrophotometry (Mg and Ca) and ion chromatography (F, Cl, and S), and measurements are in parts per million. Analytical error is ≤5% except for samples D1 and F1, for which it is ~20%. Location of stratigraphic sections is as follows: C is at Matalau (2.3 km northeast of Rabaul town), D is at the airport terminal (immediately south of Rabaul town), and F is 2 km northwest of the Tavurvur crater. Depositional units correlate between the three sections. Sections C and F were scaled to section D to account for variable section thickness.

Sample	Stratigraphic position (cm)	Mg	Ca	F	Cl	S
F1	42	5	220	25	469	397
D1	37	515	650	366	5232	684
D2	32	22	582	29	182	494
D3	27.5	8	57	0	93	109
D4	24.5	8	608	15	134	529
D5	22	11	594	6	125	519
D6	21	8	602	39	109	538
D7	19	12	598	3	92	542
D8	17	39	594	33	196	604
D9	15.5	28	602	13	205	575
F7	15	15	576	6	20	494
D10	14.5	47	657	11	148	602
D11*	13	34	310	0	182	340
D12*	8.5	52	111	0	280	177
D13*	2.5	98	162	0	1242	239
C9	0.5	72	590	0	360	624

*Ash from Vulcan; others are from Tavurvur.

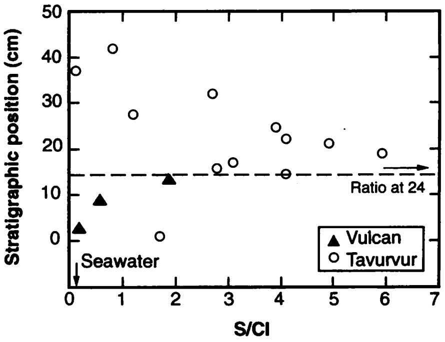

Fig. 2. Ash leachate data from the 1994 eruption of Rabaul. The dashed line shows the depositional break between Vulcan ash below (triangles) and Tavurvur ash above (circles) (seawater S is 2712 ppm and Cl is 19353 ppm) (*4*).

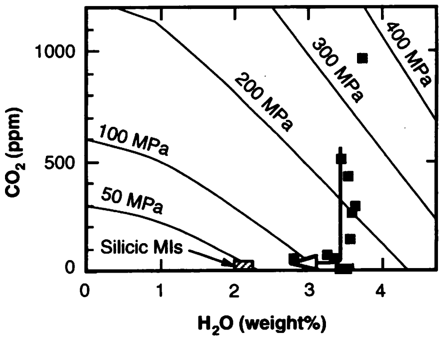

Fig. 3. CO_2-H_2O contents of mafic MIs (solid squares). Lines are fluid-saturation isobars (50 to 400 MPa) (*18*).

to represent xenocrysts because of their mineral compositions (*6*). The olivine crystals, which are particularly common in Tavurvur ash, are euhedral and lack reaction rims. Our analyses of Tavurvur olivine MIs reveal a genetic association with the 1994 eruption. The composition of the olivine MIs ranges from a basalt to a basaltic andesite (48.4 to 53.5 weight % SiO_2), which is similar to that of other deposits from the complex (*7, 8*). Early erupted ash contains the most evolved olivine MIs, whereas later erupted ash has less evolved MIs (lower MgO and higher K_2O). Volatile elements in olivine MIs also correlate with stratigraphy, with early erupted more evolved MIs having lower volatile contents than later erupted less evolved MIs (Table 3 and Fig. 3).

The compositional similarity of bulk ash, MG, and MIs from Vulcan and Tavurvur suggests derivation from a single magma chamber (*6*) (Table 2). The sequential eruption of less evolved MG and MI compositions at Rabaul is consistent with the tapping of a compositionally stratified magma chamber. Minimum depth estimates based on silicic MI volatile contents (1.5 km) (*9*) are similar to estimates from earthquake activity during unrest between 1983 and 1985. Hypocenters define a large elliptical ring centered on the Rabaul caldera, dipping outward and extending beneath Vulcan and Tavurvur at 4 ± 2 km depth (Fig. 4) (*10*). Mori *et al.* (*10*) interpreted the elliptical ring as a fracture zone and, on the basis of uplift and microgravity change, suggested that magma was at a high level (~2 km) within the ring. This geometry requires lateral magma flow across the fracture zone to feed the conduits of Vulcan and Tavurvur (*10*). Although mafic magma may laterally traverse the crust in some

Table 3. Analytical data for melt inclusions from the Rabaul caldera. Host composition was measured within 10 μm of the MI or rim. MI volatiles were determined by infrared spectroscopy with the use of published extinction coefficients (*20*). The detection limit for CO_2 in mafic and silicic MIs is 50 to 100 ppm, depending on spectra quality, with relative precision varying from 15% at moderate abundance (~250 ppm) to 10% at higher levels (>400 ppm). Water uncertainty is <10% relative. Abbreviations: M, mafic MI hosted by olivine; S, silicic MI hosted by orthopyroxene; b.d.l., below detection limit; and ND, not determined. Numbers in parentheses indicate percent analytical error.

MI	Type	Host composition (Mg#)		Stratigraphic position (cm)	H_2O (weight %)	CO_2 (ppm)
		Near MI	Rim			
F1-1	M	85.6	ND	40	3.8	960 (6)
F1-2a	M	ND	ND	40	3.7	290 (14)
F3-1	M	84.2	83.7	35	3.4	b.d.l.
F3-2	M	85.8	ND	35	3.5	510 (10)
F4-3a*	M	84.6	84.6	30	3.5	b.d.l.
F4-3b*	M	84.6	84.6	30	3.6	420 (10)
F4-4	M	85.4	ND	30	3.6	250 (20)
F6-2	M	82.3	74.8	20	3.6	130 (18)
F6-3	M	84.2	83.4	20	3.3	70 (40)
F8-1	M	83.6	76.5	13	3.4	50 (70)
F8-2	M	81.9	81.8	13	2.8	50 (70)
D12C-2†	S	ND	ND	8.5	2.3	b.d.l.
D12B-4†	S	ND	ND	8.5	2.3	b.d.l.
D13-1†	S	ND	ND	2.5	2.2	b.d.l.
D13-2†	S	ND	ND	2.5	2.0	b.d.l.
RB1-1a‡	S	ND	ND	ND	2.2	b.d.l.
RB2-1a‡	S	ND	ND	ND	2.5	b.d.l.

*Compositionally identical MI within same crystal (F4-3a has probably leaked CO_2). †From Vulcan. ‡From 1400-year-old eruption; others are from Tavurvur.

Table 2. Major element analyses of bulk rock, MIs, and MG from Rabaul. All analyses were normalized to 100% on a volatile-free basis; total iron is reported as FeO. Bulk rock analyses were determined by x-ray fluorescence on fused lithium tetraborate disks. The three bulk analyses are of handpicked grain separates from Tavurvur ash (B, dense black glass chips; G, gray, poorly vesiculated grains; V, black scoria). MI and MG analyses were determined by an electron microprobe with a 20-μm beam, 15-keV accelerating voltage, and 10-nA beam current. Na was counted first in the analysis cycle, and on-peak counting times were limited to 10 s to minimize Na loss. The following percent standard deviations were based on counting statistics: SiO_2 (1), TiO_2 (4), Al_2O_3 (1.5), FeO (4), MnO (25), MgO (5), CaO (2), Na_2O (4), K_2O (4), P_2O_5 (25), SO_3 (50), and Cl (10). Measurements shown are in weight % oxide. Abbreviations: ND, not determined; S, silicic; and M, mafic.

Sample	Type	Stratigraphic position (cm)	Analyses (*n*)	SiO_2	TiO_2	Al_2O_3	FeO	MnO	MgO	CaO	Na_2O	K_2O	P_2O_5	SO_3	Cl	Original total
F1-B	Bulk	40	1	61.66	0.92	15.99	6.03	0.17	2.52	5.59	4.45	2.34	0.33	ND	ND	99.20
F1-G	Bulk	40	1	61.40	1.00	16.13	5.85	0.17	2.70	5.75	4.38	2.29	0.33	ND	ND	99.58
F1-V	Bulk	40	1	61.31	0.90	16.18	5.81	0.16	2.81	5.79	4.44	2.29	0.32	ND	ND	100.08
F1	S MI	40	3	67.02	0.80	14.81	5.06	0.14	1.29	2.77	4.67	3.20	0.26	0.05	0.39	98.23
F4	S MI	30	3	65.36	0.83	15.30	5.15	0.17	1.46	3.59	5.10	2.85	0.21	0.11	0.34	98.86
F6	S MI	20	5	64.59	0.86	15.67	5.59	0.16	1.62	3.95	4.49	2.73	0.33	0.09	0.37	97.38
F8	S MI	13	4	65.16	0.86	15.29	5.62	0.16	1.37	3.80	4.71	2.73	0.32	0.08	0.30	97.90
D12*	S MI	8.5	8	66.93	0.81	15.25	4.82	0.14	1.24	3.27	4.35	2.92	0.26	0.05	0.32	97.84
D13*	S MI	2.5	2	68.03	0.82	15.09	4.13	0.16	1.11	2.98	4.34	3.15	0.19	0.04	0.35	97.32
RB†	S MI	ND	3	68.73	0.74	15.14	3.79	0.13	0.90	2.57	4.68	3.09	0.22	0.04	0.29	97.17
F1	MG	40	4	67.87	0.80	15.11	4.12	0.12	0.95	2.79	4.78	3.26	0.21	0.00	0.29	98.84
F4	MG	30	2	64.14	0.89	15.45	5.91	0.17	1.71	4.23	4.49	2.76	0.27	0.03	0.26	100.15
F6	MG	20	2	63.87	0.84	16.18	5.60	0.15	1.49	4.59	4.36	2.61	0.31	0.00	0.25	99.73
F8	MG	13	5	65.74	0.84	15.31	5.16	0.16	1.45	3.68	4.49	2.87	0.29	0.04	0.30	99.05
D12*	MG	8.5	13	65.52	0.78	16.15	4.68	0.13	1.23	3.94	4.58	2.77	0.21	0.05	0.30	99.40
D13*	MG	2.5	2	68.21	0.77	15.15	3.86	0.07	0.99	2.77	4.71	3.22	0.26	0.00	0.29	98.28
RB†	MG	ND	4	68.07	0.76	15.13	3.77	0.13	1.02	2.90	4.90	3.08	0.24	0.09	0.31	99.42
F1-2a	M MI	40	1	48.54	0.99	18.71	9.57	0.20	4.89	13.97	2.45	0.56	0.11	0.16	0.10	96.11
F8-2	M MI	13	1	53.61	0.99	18.05	8.21	0.16	2.74	11.89	3.18	1.00	0.19	0.10	0.11	96.63

*From Vulcan. †1400-year-old eruption; all other analyses are from Tavurvur.

cases (*11*), the viscosity of Rabaul's andesite melt suggests that lateral magma flow from a central region is unlikely. We speculate that the magma erupted at Vulcan and Tavurvur rose vertically to the volcanoes from a large chamber below the seismic annulus.

Given that Vulcan and Tavurvur tapped the same magma chamber, their contrasting eruptive style can be attributed to volatile content and vent geometry. The silicic MIs from Vulcan show that the melt had 2 to 2.3 weight % water at the time of entrapment. Higher melt volatile contents are possible if crystallization drove volatile enrichment after MI entrapment, but the similarity between MG and silicic MI compositions suggests that little crystallization occurred after MI entrapment. More volatiles may have been present as a separate gas phase (*12*) and Vulcan, which erupted the most evolved magma, based on MI and MG compositions, probably tapped the volatile-rich top of the chamber.

The emission of 26 kton/day of SO_2 at Tavurvur 10 days after the plinian eruption is one of the largest fluxes ever measured during low-level eruptive activity (*13*). The flux represents the passive degassing of either a large volume of melt or a S-rich mafic melt. Mafic melt that supplied the SO_2 may have also been the source of the mafic crystal assemblage. The close compositional-stratigraphic relations of MIs indicate that olivine crystallized from a single magma batch and H_2O-CO_2 variation resembles that caused by decompression degassing (Fig. 3). Crystallization of a fluid-saturated melt during ascent (~2.5 to 7 km depth) (*14*) through a dike could account for H_2O-CO_2 variation in the MIs. Magma ascent rates would have to be slow enough to allow cooling and crystallization but fast enough to offset crystal settling (10 cm/s to 10^{-2} cm/s) (*15*).

The presence of mafic melt in large silicic systems is not unusual; however, at Rabaul, the question remains as to how olivine crystals became entrained in the andesite erupted from Vulcan and Tavurvur. The crystals might be remnants of rapid crystallization (*16*), but this requires a large amount of crystallization (~50%), efficient removal of the newly formed crystals, and coincident retention of olivine, magnesian clinopyroxene, and calcic plagioclase in the erupting magma. Alternatively, mafic melt entering the silicic magma chamber could have melted a large quantity of dacite (the composition of 1994 MG), but this model is difficult to reconcile with bulk ash homogeneity (Table 2) and the compositional similarity of silicic MIs and MG. Magma mixing is one explanation for the olivine MI relations although, with the exception of minor transition metal (Ni and Sc) variation, mixing features have not been identified in the 1994 eruptive products (*6*). Compositional agreement between silicic MI and MG compositions (Table 2) suggests that either the amount of mixing was very small or that mixing occurred before silicic MI entrapment.

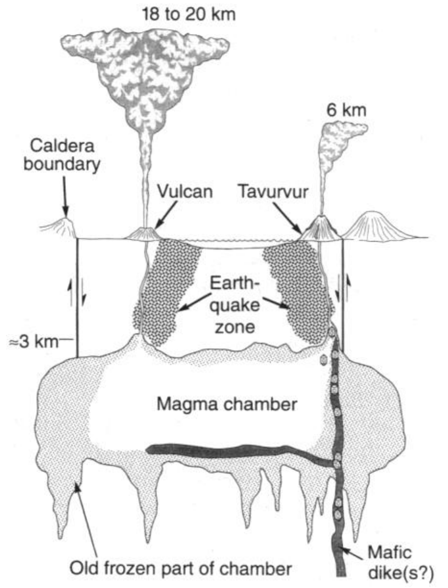

Fig. 4. Schematic cross section of the Rabaul magmatic complex. Features such as volcanic cones, dike width, and crystals have been exaggerated to show detail. A mafic dike carrying olivine crystals is represented by a filled pattern. The outward dipping fracture zone (dark stippled area) was drawn approximately based on seismicity (*10*).

REFERENCES AND NOTES

1. R. Blong and C. McKee, *The Rabaul Eruption 1994: Destruction of a Town* (Natural Hazards Research Centre, Macquarie University, Australia, 1995).
2. Although it was reported [W. I. Rose *et al.*, *Nature* **375**, 477 (1995)] that the TOMS detected SO_2 in the Rabaul eruption plume for 5 days, beginning on the day of the eruption (19 September 1994), there was no detectable SO_2 on the first day of the eruption [C. O. McKee *et al.*, *Global Volcan. Net. Bull.* **19**, 2 (1994)].
3. I. E. Sprod, personal communication.
4. M. S. Quimby-Hunt and K. K. Turekian, *Eos* **64**, 130 (1983).
5. Typical mafic ash leachate S/Cl values for the Cerro Negro volcano in Nicaragua are ~1 to 7 [W. I. Rose, *Geology* **5**, 621 (1977)]. The average S/Cl ratio for the dacitic 1980 Mount St. Helen eruption was 0.66, with S ~650 ppm [R. E. Stoiber, S. N. Williams, L. L. Malinconico Jr., D. A. Johnston, T. J. Casadevall, *J. Volcanol. Geotherm. Res.* **11**, 203 (1981)]. The high S/Cl ratios of Tavurvur ash could reflect a high oxidation state or the presence of a mafic melt in the magma chamber, or both.
6. R. W. Johnson *et al.*, *Eos* **76**, 171 (1995). Reported xenocryst compositions from the 1994 ash are as follows: Tavurvur ash, olivine Mg# 78 to 84, plagioclase An$_{80-93}$, and clinopyroxene Mg# 82 to 85; Mg# = 100 Mg/(Mg + Fe) atomic; Vulcan ash, olivine Mg# 75 to 80, and plagioclase An$_{60-75}$.
7. Fe-Mg crystal-melt partitioning indicates that olivine post-entrapment crystallization was minor (0 to 7%). MI compositions were first adjusted with the use of the empirical relation of A. Kilinc, I. S. E. Carmichael, M. L. Rivers, and R. O. Sack [*Contrib. Mineral. Petrol.* **83**, 136 (1983)] and bulk rock ferrous/ferric data [R. F. Heming, *Geol. Soc. Am. Bull.* **85**, 1253 (1974)]. Adjusted MI compositions were compared with host olivine compositions (Table 3) with the use of the Fe-Mg distribution coefficient of P. L. Roeder and R. F. Emslie [*Contrib. Mineral. Petrol.* **29**, 275 (1970)]. The compositional variation of olivine MIs is consistent with fractional crystallization of the observed crystal assemblage.
8. C. P. Wood, I. A. Nairn, C. O. McKee, B. Talai, *J. Volcanol. Geotherm. Res.* **69**, 285 (1995).
9. C. W. Burnham, in *Volatiles in Magmas*, M. R. Carroll and J. R. Holloway, Eds., vol. 30 of *Reviews in Mineralogy* (Mineralogical Society of America, Washington, DC, 1994), pp. 123–129.
10. J. Mori *et al.*, in *Volcanic Hazards: Assessment and Monitoring*, J. H. Latter, Ed. (IAVCEI Proceedings in Volcanology, Springer-Verlag, Berlin, 1989), pp. 429–462; C. McKee, J. Mori, B. Talai, *ibid.*, pp. 399–428.
11. P. Einarsson and B. Brandsdottir, *J. Geophys. Res.* **47**, 160 (1980).
12. P. J. Wallace, A. T. Anderson Jr., A. M. Davis, *Nature* **377**, 612 (1995).
13. W. I. Rose *et al.*, *J. Geophys. Res.* **93**, 4485 (1988).
14. Olivine MI sample F1-1 has the highest saturation pressure (350 MPa) but is compositionally intermediate to other olivine MIs, which indicates that this MI is not related to the other MIs by decompression and crystallization.
15. A. R. McBirney and T. Murase, *Annu. Rev. Earth Planet. Sci.* **12**, 337 (1984); F. Spera, in *Physics of Magmatic Processes*, R. B. Hargraves, Ed. (Princeton Univ. Press, Princeton, NJ, 1980), pp. 265–323.
16. T. L. Grove and J. M. Donnelly-Nolan, *Contrib. Mineral. Petrol.* **92**, 281 (1986).
17. T. R. Alpha and H. G. Greene, *U.S. Geol. Surv. Misc. Field Stud. Map MF 1778* (1985).
18. Volatile solubilities were from J. R. Holloway and J. G. Blank, in *Volatiles in Magmas*, M. R. Carroll and J. R. Holloway, Eds., vol. 30 of *Reviews in Mineralogy* (Mineralogical Society of America, Washington, DC, 1994), pp. 187–230. The theoretical degassing trend was calculated with computer code provided by J. R. Holloway (personal communication). MI volatile leakage could mimic the degassing trend, although the correlation between saturation pressures and MI compositions (see Table 3) is consistent with crystallization during decompression. Many MIs contain vapor bubbles; vapor partitioning of CO_2 could result in underestimation of saturation pressure [A. T. Anderson Jr. and G. G. Brown, *Am. Mineral.* **78**, 794, 1993].
19. P. S. Taylor and R. E. Stoiber, *Geol. Soc. Am. Bull.* **84**, 1031 (1973).
20. G. Fine and E. Stolper, *Earth Planet. Sci. Lett.* **76**, 263 (1986); P. F. Dobson, S. Epstein, E. M. Stolper, *Geochim. Cosmochim. Acta* **53**, 2723 (1989); J. E. Dixon, E. M. Stolper, J. R. Holloway, *J. Petrol.* **36**, 1607 (1995). Assumed glass density was 2800 g/liter for mafic MIs and 2350 g/liter for silicic MIs. Water concentrations were determined by measurement of the absorption peak near 3500 cm^{-1} (except sample F3-2, for which near-infrared was measured). Backgrounds were drawn visually. In the case of mafic MIs, the spectra from hydrous CO_3-free glasses were used to reference backgrounds on compositionally similar MIs. For further discussion of Fourier transform infrared (FTIR) spectroscopy methods and associated analytical error, see P. D. Ihinger, R. L. Hervig, and P. F. McMillan, in *Volatiles in Magmas*, M. R. Carroll and J. R. Holloway, Eds., vol. 30 of *Reviews in Mineralogy* (Mineralogical Society of America, Washington, DC, 1994), pp. 67–121.
21. Thanks to Rabaul Volcano Observatory, and especially C. McKee, for assistance with field work during the eruption; J. Lowenstern of the U.S. Geological Survey for help with FTIR spectroscopy and the use of his lab; J. Clark for assisting with electron microprobe analyses (instrument support from EAR 8408163); and S. Selkirk for figure preparation. Financial support was provided by NSF grant EAR95-10188, Arizona State University, and the Lende Foundation.

13 February 1996; accepted 29 May 1996